Thermal Conductivity of Solid Deuterium by the 3ω Method

Introduction

Targets for inertial confinement fusion (ICF) require layers of solid D_2 or DT that have been formed and smoothed by sublimation and recondensation.[1] This "layering" process,[2,3] which typically takes hours, can result in a variety of internal structures in the layer that constitute departures from the desired uniformity of the layer. Knowing the thermal conductivity of the layer and how changes in structure may alter the conductivity are important to modeling the layering process.[4] Although the layering process is most easily accomplished at a temperature just below the triple point, optimizing the internal gas density of the target for ICF requires a temperature ~1.5 K below the triple point.[5] Lowering the temperature after obtaining a uniform layer can result in significant thermal contraction of the layer. This contraction can produce stresses and cracks because the solid D_2 is not free-standing but is attached to a plastic spherical surface.

A critical requirement for ICF experiments is achieving a uniformly thick shell of ice inside a spherical capsule. Analysis of the crystalline structure shows this ice layer to be hexagonally close-packed.[6] In this ice configuration heat is conducted radially out of the sphere along the *a* plane of the crystal over most of the sphere, and along the *c* axis over the remainder of the sphere. Should the thermal conduction along the *c* axis and the *a* plane be significantly different, the ice layer would have an intrinsic limit as to how uniform it could be.

In the 3ω method of measuring thermal conductivity, a wire or strip line whose resistivity is a strong function of temperature is employed as both the heater and the temperature sensor.[7–11] A sinusoidal current with angular frequency $\omega = 2\pi f$ passes through a wire or strip line that is embedded in or thermally anchored to the medium whose thermal conductivity is to be measured. Heat generated in the wire is proportional to the square of the current and therefore has a frequency component at 2ω in addition to a steady-state component, resulting in a temperature with an oscillating component at 2ω. If the wire is a high-purity metal such as Pt, its resistance varies strongly with temperature (for the wire used here, the resistance variation is 5% to 7% per K). Accordingly, the resistance also has an oscillating component at frequency 2ω. The resulting voltage between two points on the wire (the product of current at frequency ω and resistance) therefore has a component of amplitude V_ω at frequency ω and a small component of amplitude $\tilde{V}_{3\omega}$ at frequency 3ω. [See Eqs. (6)−(9) of Ref. 8.] The component $\tilde{V}_{3\omega}$ is expressed as a complex amplitude to take into account the phase shift (with respect to the fundamental, after tripling its frequency) resulting from thermal inertia in the wire and in the medium. It is straightforward to show that the amplitude $\tilde{T}$ of temperature variation in the wire is proportional to $\tilde{V}_{3\omega}$,

$$\tilde{T} = 2\frac{\tilde{V}_{3\omega}}{V_\omega}\frac{R}{\mathrm{d}R/\mathrm{d}T}, \tag{1}$$

where R is the resistance of the wire (between the voltage leads) at the ambient temperature T. Equation (1) is equivalent to Eq. (12) of Cahill (as corrected in the erratum)[7] and is implicitly given in Eq. (9) of Birge *et al.*[8] This equation is valid even if there is a small temperature variation along the wire and, in that case, gives the average temperature amplitude. Since the temperature amplitude $\tilde{T}$ depends strongly on the amount of heat conducted away by the medium, it can be used as a measure of the thermal conductivity of the medium. By making the wire one arm of a bridge circuit, sensitivity to V_ω is minimized and $\tilde{V}_{3\omega}$ can be amplified and measured with a lock-in amplifier. In this work, the principal source of error is noise in the first stage of amplification, which is partially overcome by using the lock-in amplifier to achieve a narrow bandwidth and a long averaging time.

Cahill introduced the useful concept of "thermal penetration depth," which gives an estimate of the distance that a temperature oscillation penetrates into the medium. This quantity is given by $\left[\kappa/(2\rho\omega C)\right]^{1/2}$, where κ is the thermal conductivity in the medium, ρ is the density, and C is the specific heat.[7] This indicator of how far the wire must be from other parts of the apparatus is in agreement with temperature distributions in the medium calculated by the numerical model described in **Numerical Model**, p. 51.

A more-conventional method for measuring thermal conductivity is imposing a thermal gradient on a bulk sample and measuring the resulting heat flow. A drawback to this method for D_2 is the shrinkage (a 14% increase in density upon solidification and an additional 3% upon cooling from the triple point to 10 K) pulling the medium out of contact with one of the heating or sensing elements. This problem was discussed by Collins *et al.*[12] and Souers.[13] Daney[14] overcame this problem by observing the rate of ice growth on a cooled rod immersed in liquid and inferring the thermal conductivity from that rate. In the method used here, the solid forms around a wire of very small diameter (15 μm). Shrinkage upon further cooling may produce stresses in the solid D_2, but it is not expected to pull the D_2 away from the wire. This expectation is confirmed by observation [see later in Fig. 129.60(c)]. Conventional measurements of the thermal conductivity of liquid are subject to errors caused by convection. The high-frequency method used here should be virtually immune to convection issues.

Some proposed targets for ICF use solid D_2 or DT inside low-density polymer foam. Liquid D_2 soaks readily into such foams,[15] and it was found (using silica aerogel foam) by Daney and Mapoles[16] that the thermal conductivity of liquid in foam is very close to that of liquid by itself. When the liquid solidifies, voids may develop that affect both the thermal conductivity and the performance of ICF foam targets. The presence of a sizeable void content could be confirmed by embedding a wire in the foam and measuring its thermal conductivity by the 3ω method.

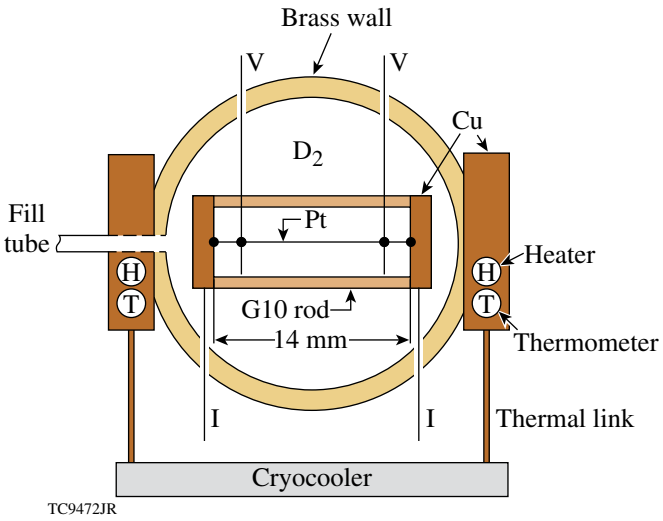

Figure 129.55
Apparatus employed to measure the thermal conductivity of D_2. Glass windows parallel to the plane of this figure allow one to observe the condensation and solidification process. The Pt wire is 1.0 mm from one window, 1.8 mm from the other window, and 2.8 mm from the G10 rods. Copper blocks on either side of the brass chamber have heaters (H) and thermometers (T) that allow one to impose a thermal gradient during the solidification process. Thermal links to the cryocooler are sized to provide adequate cooling, while allowing for a sufficient thermal gradient during the solidification process. The voltage leads (V) and current leads (I) exit the chamber through vacuum feedthroughs.

Experimental Setup

The active element used in this work is a 15.0±0.2-μm-diam Pt wire (measured by a scanning electron microscope). The wire is annealed and is of 99.99% purity.[17] As shown in Fig. 129.55, the Pt wire is soldered to Cu blocks 14 mm apart and attached to voltage leads (25-μm-diam stainless steel). The Cu blocks are held apart by G10 rods (insulating polymer-glass composite) that also provide support for the voltage leads. The voltage leads are attached to points on the Pt wire ~10 mm apart, either with solder or electrically conductive epoxy. Care is taken to avoid flexing or stretching of the Pt wire and to minimize the mass of the connection to the voltage leads. To minimize stresses on the Pt wire, a three-axis positioner is used to mount the Pt wire and to solder the voltage leads to it. After assembly, the distances between the attachment points are precisely measured using a micrometer stage under a microscope. Although the stainless steel of the voltage leads is more thermally conductive than the D_2 (by a factor of ~6 for solid D_2 at the triple point), its heat capacity is small and its thermal conductivity is a factor of ~30 smaller than that of the Pt. The voltage leads are assumed not to be a significant thermal perturbation to the experiment.

The resistance R of the Pt wire was measured as a function of temperature (T), since an accurate knowledge of $R/(\mathrm{d}R/\mathrm{d}T)$ is required to determine the temperature amplitude. A third-order polynomial provides a good fit to the resistance as a function of temperature, as seen in Fig. 129.56. Of five Pt wires used at different times, three agreed in resistance per unit length over the experimental temperature range (11 K to 26 K), while two wires showed slightly greater resistance. It is likely that mechanical flexing and stretching in the course of mounting these delicate wires sometimes resulted in increased resistance. In one instance, the wire was noticeably deformed by the rapid melting of solid D_2 and thereafter exhibited increased resistance. The thermal conductivity of the Pt wire as a function of temperature is obtained from the Metalpak program of Arp,[18] based on the residual resistance ratio (RRR) of the Pt wire (i.e., the ratio of resistance at 273 K to the resistance at a temperature ≤4 K). The value of RRR was determined by measuring the ratios of resistance at 294 K to the resistance values in the range 14 K to 18 K and comparing these ratios to the corresponding ratios given by Ref. 18. This procedure

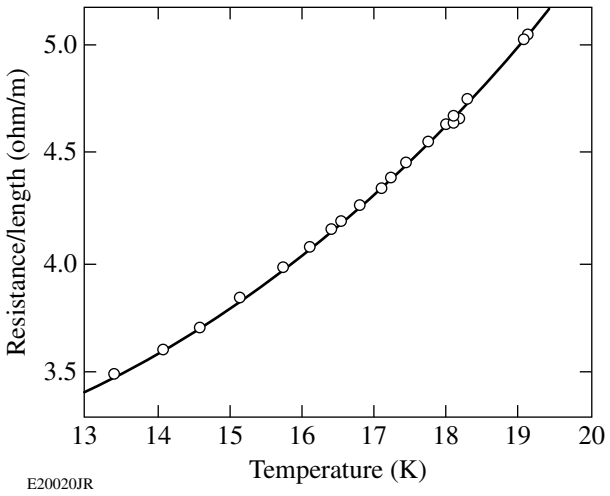

Figure 129.56
Resistance per unit length of a Pt wire as a function of temperature. The measured data are fit with a third-order polynomial.

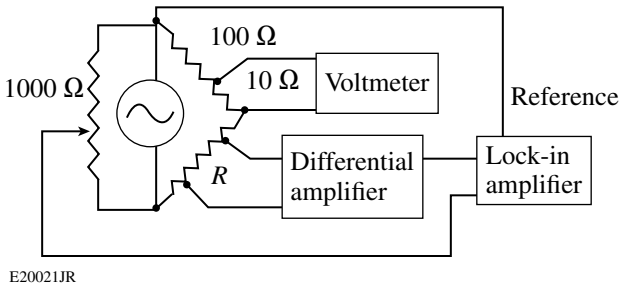

Figure 129.57
Circuit for measuring thermal conductivity. The voltmeter monitors current through the Pt-wire sample resistance *R*. The bridge is balanced with the lock-in amplifier set to detect the fundamental frequency, and the output of the oscillator (which is internal to the lock-in amplifier) is attenuated. After balancing the bridge at a single frequency, the lock-in amplifier is reset to detect the third harmonic. A LabVIEW program collects and averages data at a series of frequencies. No bandwidth limitations are imposed in amplification since these would produce phase shifts. The differential amplifier is Stanford Research Systems model SR560, and the lock-in amplifier (which also uses a differential input) is model SR830.

yields RRR = 186 to 196 and Pt conductivity values ranging from 350 W/(m K) at 18 K to 410 W/(m K) at 14 K. The range of values for RRR produces ≤2% uncertainty in the Pt thermal conductivity values and does not add any uncertainty to the thermal conductivity values obtained for solid D_2.

The chamber in Fig. 129.55 consists of a vacuum-tight brass cylinder with electrical feedthroughs soldered in and glass windows sealed to the chamber by compression of indium gaskets. The windows allow one to backlight and image the D_2 liquid or solid. Materials were chosen that would provide the thermal gradients necessary to fill the chamber with solid deuterium. Copper blocks of high purity on each side of the brass cylinder have very high thermal conductivity compared with the brass and glass (by a factor of >10) and facilitate establishing and measuring the thermal gradient. The experimental chamber is thermally linked to the cold finger of the cryostat. The thermal links are somewhat weak to allow one to impose a thermal gradient, using heaters. After the heaters are turned off and temperatures stabilize, a small thermal gradient of ~0.2 K/cm remains in the region of the apparatus containing the Pt wire. This gradient is a consequence of the necessary weakness of the thermal links to the cold finger and not a significant source of experimental error. The experimental chamber is surrounded by a copper radiation shield at 40 K. Windows in the radiation shield are coated with ~10 nm of Au to reduce thermal radiation coming into the chamber.

The electrical configuration is shown in Fig. 129.57. After stabilizing the temperature in the D_2, the resistance of the Pt wire between the voltage leads is determined. The bridge circuit is then balanced by manually adjusting the variable resistor, while the lock-in amplifier is set to detect the fundamental frequency of the sine-wave oscillator. A single frequency is used to determine resistance and balance the bridge; these functions are found to be insensitive to the choice of this frequency. The oscillator, internal to the lock-in amplifier, is of high spectral purity, with harmonic distortion of −80 dB (Ref. 19). It is assumed that any component of distortion at frequency 3ω is partially removed by balancing the bridge. Replacing the Pt wire by a Cu wire at room temperature with a similar resistance demonstrates that the influence of oscillator distortion is insignificant. Some measured values of $\tilde{V}_{3\omega}$ for solid D_2 at <17 K are as small as 17 nV (rms), which is 96 dB below the value of V_{ω}, i.e., 1.1 mV (rms).

To obtain a value of thermal conductivity, the third-harmonic voltage $\tilde{V}_{3\omega}$ is measured as a function of frequency. Each value of voltage is recorded as a complex number, the values in phase or out of phase with the driving current. Holding the ambient temperature constant, data are taken at a series of frequencies increasing at logarithmic intervals from ~1 Hz to >1000 Hz. This scan typically takes 2 to 20 min and is repeated to ensure that the state of the solid D_2 has not changed. The data at each frequency are averaged, after an initial settling time that is governed by the time constant selected on the lock-in amplifier. Some scans are rejected after finding that the state of the solid D_2 has apparently changed between the first and second scans. Non-repeatable scans are found to be especially likely if there is a visible crack or cavity somewhere in the solid D_2.

In such a case, heat generated in the Pt wire hollows out a new cavity around the wire itself, and the gas that is generated is able to find a path to the original cavity and recondense there. When large enough, a cavity around the wire becomes visible through a microscope with an attached video camera. When a cavity develops around the wire, there is a sudden rise in the in-phase temperature amplitude, and the data are rejected.

Data are fitted with the two-dimensional (2-D) numerical model described in **Numerical Model**, which includes, as input parameters, the dimensions of the wire and the medium, the density, specific heat and thermal conductivity of Pt,[18] and the density,[20] specific heat,[21,22] and thermal conductivity of D_2. The latter five parameters are highly temperature dependent. The only fitting parameter is the thermal conductivity of the D_2 since the other parameters are presumed to be known to sufficient accuracy. At the temperatures employed here, the heat capacity per unit volume of the liquid or solid D_2 is a factor of 4 to 7 greater than that of the wire. These ratios, much greater than those often found with other materials at higher temperatures, facilitate the measurement by overcoming the loss of sensitivity resulting from the very small wire resistance. If the voltage leads are located sufficiently far from the ends of the wire, the numerical model yields results very close to the analytical solution [Eq. (21)] of Chen *et al.*[9] for a one-dimensional (1-D) problem where it is assumed that the wire is infinitely long (i.e., no heat flow in the direction of the axis of the wire) and that the wire has a much greater thermal conductivity than the surrounding medium.

To maintain purity of the D_2 against possible contamination by air or other gases, impurities are removed with each cryogenic cycle. Between uses, the D_2 is stored as a room-temperature gas at ~1 atm. After condensing the D_2 in the experimental chamber and taking data, the chamber is warmed to ~30 K, evaporating the D_2, but leaving residual air (if any) frozen. After isolating the D_2 and warming the apparatus, the contaminants are pumped away.

For some of the data, the D_2 was converted from normal D_2 to ortho D_2 using a catalyst. To achieve this conversion, the D_2 was first condensed into a separate chamber of volume 5 cm^3 containing 2 g of hydrated iron oxide[23] (catalyst grade, 30/50 mesh). Prior to cooling, the catalyst was baked in vacuum (150°C for ~2 h, until the outgassing rate became small). The D_2 was kept in this chamber for several days as liquid just above the triple point, while the adjacent experimental chamber was kept several K higher to prevent any condensation there. After several days, it was presumed that all the D_2 had been converted[24] to ortho D_2. Some of the D_2 was then distilled into the experimental chamber (volume 0.9 cm^3) by reversing the relative temperatures of the two chambers.

Numerical Model

A computer program modeled this experiment to relate the measured temperature amplitude to the thermal conductivity in the medium. The model takes into account the 2-D geometry of the experiment and includes thermal conduction along the wire, as well as conduction in the medium both perpendicular and parallel to the wire. This model has been used to determine the significance of 2-D effects and to provide improved accuracy over 1-D numerical solutions, which ignore heat flow in the direction of the wire axis.

The 2-D domain used by the model is shown in Fig. 129.58. The model assumes a cylindrically symmetric (r,z) geometry consisting of the wire, the medium, and surrounding heat baths. While the distance from the wire to the boundary varies from 1 to 3 mm in the experiment (see Fig. 129.55), the cylindrical geometry is valid for all but the lowest frequencies because the oscillating temperature T falls to zero within distances significantly less than 1 mm. The radius of the wire (7.5 μm) is small when compared with the radial width of the outer boundary (1 mm); therefore, a variable-size grid was implemented in the medium, wherein the radial widths of the cells increase geometrically with their distance from the wire. The cell widths in z are kept uniform for all media. The model is similar to that presented in Jacquot *et al.*,[25] who performed

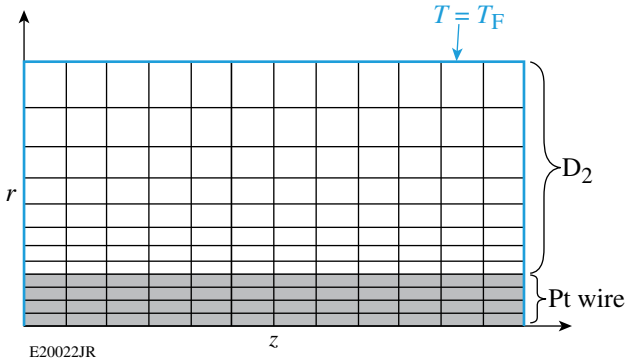

Figure 129.58
Schematic of the 2-D domain used by the numerical code. The Pt wire (shaded region) is fine zoned in the radial direction, matched to variable zoning in the D_2. Azimuthal symmetry is assumed with a fixed temperature $T = T_F$ specified on each of the three boundaries. An oscillatory current is applied uniformly through the wire. The code solves a 2-D diffusion equation for the complex 2ω temperature component.

initial-value heat-flow calculations in a different geometry for a 3ω experiment using a rectangular metal strip as the heater placed on top of the sample.

To achieve accurate solutions, 50 uniformly spaced cells were used in the axial direction, with >400 uniformly spaced radial cells in the wire and 1300 geometrically spaced cells in the medium. The large number of radial cells in the wire was required to ensure continuity of cell size across the wire–medium boundary. Small cells in the medium close to the wire are required to resolve the spatial variations at high frequencies. The average of the Pt and D_2 conductivities is used at the Pt–D_2 boundary. There is no heat flux across the lower boundary of the Pt wire (the z axis). The temperature T is fixed on the three sides of the domain that are heat baths. The heat source is nonzero only for in Pt cells.

For each cell

$$\rho C \frac{\partial T}{\partial t} + \nabla \cdot Q = W \tag{2}$$

is solved, where the heat flux Q is given by $Q = -\kappa \nabla \mathrm{T}$ and W is the heat deposited in the wire per unit volume. The code can solve Eq. (2) as an initial-value problem using a conventional finite-difference technique. Energy conservation is ensured by expressing the heat flux between two cells as a quantity proportional to the difference in temperature between the cells. Implicit differencing of Eq. (2) leads to a matrix equation for the new temperature T of the form $MT = S$, where M is a five-diagonal matrix and S is a vector evaluated at the previous time step. The matrix equation is solved using Kershaw's incomplete Cholesky conjugate gradient (ICCG) method.[26] Details of the numerical implementation are given in Ref. 27. Since it would be excessively time consuming to solve the initial value problem for the present experiment, where the asymptotic second-harmonic response to the oscillating current is required, an alternative approach is used that yields the oscillating temperature amplitude $\tilde{T}(r,z)$ directly. Assuming that the current varies as $\cos(\omega t)$, the heat deposition W may be written as

$$W(t) = W_0 + \frac{1}{2}\left(\tilde{W} e^{i2\omega t} + \tilde{W} e^{-i2\omega t}\right), \tag{3}$$

where W_0 is the time-averaged deposition and $\tilde{W} = W_0$. The asymptotic temperature is then given by

$$T(r,z,t) = T_0(r,z) + \frac{1}{2}\left[\tilde{T}(r,z) e^{2i\omega t} + \tilde{T}^{*}(r,z) e^{-2i\omega t}\right], \tag{4}$$

where $T_0(r,z)$ is the steady-state solution satisfying $-\nabla \bullet (\kappa \nabla T_0) = W_0$. Inserting Eqs. (3) and (4) into Eq. (2), one finds

$$i\omega\rho C\tilde{T} - \frac{1}{2}\nabla \cdot \kappa \nabla \tilde{T} = \tilde{W}. \tag{5}$$

This equation is differenced as for the initial value solution, and $\tilde{T}(r,z) = 0$ is imposed on the physical boundaries. A similar five-diagonal matrix equation is obtained, but the central diagonal of the matrix contains complex numbers and the solution $\tilde{T}(r,z)$ is complex. It has been found[27] that Kershaw's ICCG method generalized to operate with complex numbers converges to provide the complex solution $\tilde{T}(r,z)$. Noting that the resistivity of the wire (which is linear in temperature over small-enough temperature excursions) has a second-harmonic component proportional to $\tilde{T}(r,z)$ and the resistance along the wire combines in series, it is easy to see that the third-harmonic voltage $\tilde{V}_{3\omega}$ is that given in Eq. (1), where $\tilde{T}$ is the average value of $\tilde{T}(r,z)$ between the two voltage leads. In practice, because of the high thermal conductivity and small radius of the Pt wire, the r dependence of $\tilde{T}(r,z)$ in the wire is very small and it is the z variations of $\tilde{T}(r,z)$ that determine the average.

By solving the initial value problem, it is found that the time taken for the wire to reach a constant ambient temperature in vacuum is <40 ms. Longer times are required for solid D_2, but over the several-minute averaging time of the measurement, transient effects are negligible. Figure 129.59 illustrates the use of the numerical model to obtain the spatial distribution of the temperature amplitude in the wire and in the medium. In Figs. 129.59(a) and 129.59(b), it is seen that thermal conduction along the wire reduces the temperature amplitude near the end of the wire, but that locating the voltage leads ~2 mm from the ends places them in a region of constant temperature amplitude. This constant amplitude is found to be the same (within 0.5%) as that calculated by the 1-D model [Eq. (21)] of Ref. 9. In Figs. 129.59(c) and 129.59(d), the radial temperature distribution in the wire and in the solid D_2 is shown [(c) in phase and (d) out of phase], starting from the mid-point of the wire. In Fig. 129.59(e) the in-phase temperature amplitude in the wire is magnified at a single frequency to show a 1-μK temperature drop between the center and the edge at 7.5 μm.

To understand departures of the experimental data from the numerical model, particularly at frequencies >1 KHz, two modifications were introduced. Neither of these yielded an improved fit to the observed data, but they are mentioned here as strategies available to users of the 3ω method. A thin layer of frozen air on the wire was added to the model but failed to

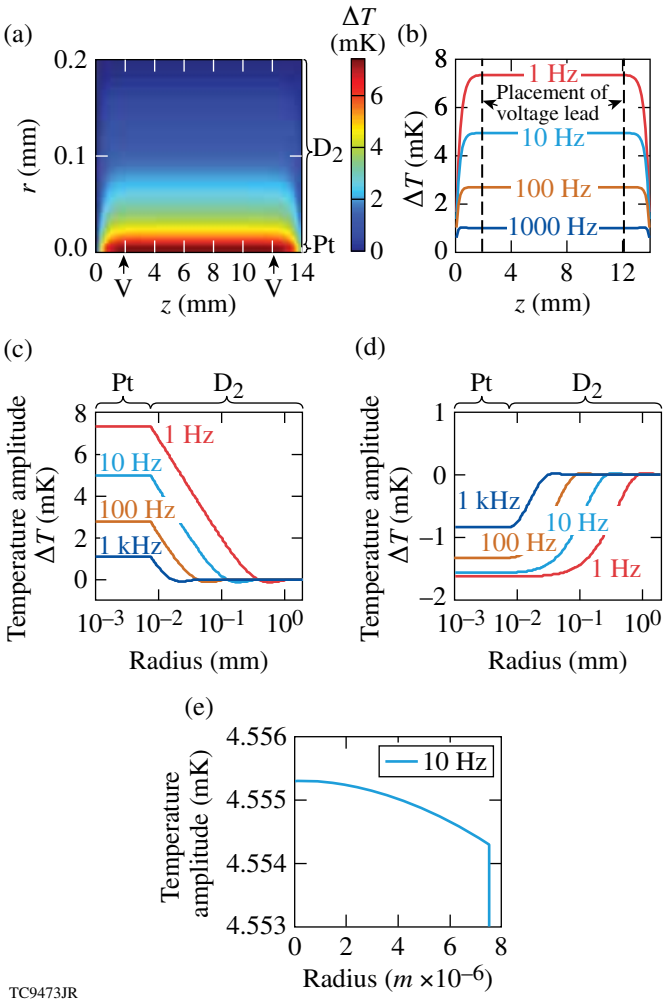

Figure 129.59
Illustrative results of the 2-D model. (a) Calculated contour plot of temperature amplitude (the in-phase component) in and around the Pt wire embedded in solid D_2 at 18 K. A sinusoidal current at 1 Hz results in dissipation of 45 μW between the voltage leads, labeled V. (b) In-phase temperature amplitude as a function of distance along the wire. (c) In-phase and (d) out-of-phase temperature amplitudes as a function of radial distance from the center of the wire starting at the mid-point of the wire. (e) Magnification of (c) showing a 1.0-μK drop in the temperature amplitude between the center and edge of the wire at 10 Hz.

improve the fit. Surface irregularities on the 1-μm level were added to the Pt wire but also failed to improve the fit.

Results

Before measurements on solid D_2 are undertaken, significant effort is required to obtain solid D_2 free of obvious cavities and cracks. The chamber is observed visually while liquid is condensing and then while solidification proceeds in the presence of an imposed thermal gradient. The solid grows slowly (over several hours) from the cold side to the warm side, with the liquid in the fill tube being the last to solidify. Because of the 14% increase in density upon solidification of the liquid D_2, gas cavities can easily be trapped in the solid. If this happens, the warm side is reheated until the cavities are filled with liquid, and the solidification process is then resumed. If cavities are allowed to remain, they can cause the thermal conductivity measurement to fail because they gradually move (by sublimation on the warm side of the cavity and recondensation on the cold side) in response to residual thermal gradients and often find their way to the Pt wire.

Before a measurement, the D_2 solid is evaluated visually as shown in Fig. 129.60. Figure 129.60(a) shows the interface between liquid and solid as the solid grows, and the resulting solid is shown in Fig. 129.60(b). Upon lowering the temperature of clear solid D_2 as seen in Fig. 129.60(b), many visual features appear, such as cracks and regions where the solid has apparently pulled slightly away from a window or the wire supports, as seen in Fig. 129.60(c). After remaining at a constant temperature for a period of several hours to a day, cracks and other features appear to heal, the solid again becomes visually clear, and a repeatable measurement of thermal conductivity can be made. The crystallinity of the solid is examined by viewing it in polarized light as shown in Figs. 129.60(d) and

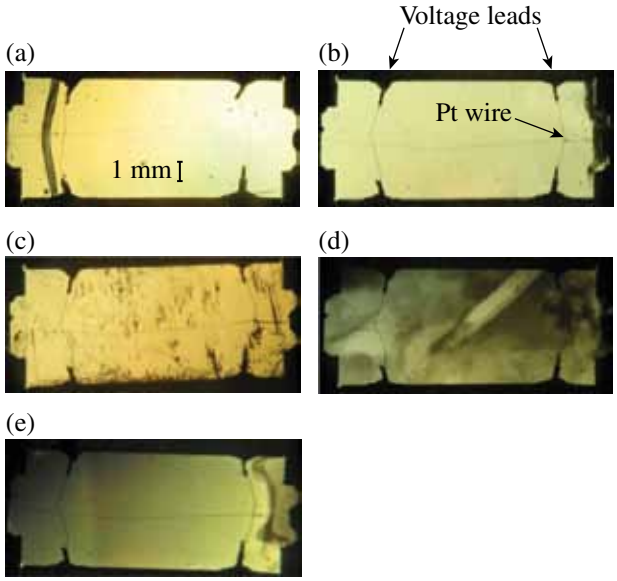

Figure 129.60
Various views of solid D_2 formed around the Pt wire and the voltage leads. (a) Solid forming on the left side with liquid on the right, in the presence of a thermal gradient. The dark line is caused by refraction at the interface between solid and liquid. (b) Solid successfully formed, free of apparent flaws. (c) Solid with cracks after suddenly lowering the temperature by 2 K. [(d) and (e)] Two examples of solid in polarized light revealing features of the crystallinity.

129.60(e). In both cases the solid was visually clear when viewed without polarizers and provided repeatable thermal conductivity data. Typically, several domains are seen, random in shape, with dimensions in the range of 1 to 8 mm. These domains are revealed by variations in color and shading as the polarizers are slowly rotated. It appears that the Pt wire passes through several large crystallites. If a single crystal could be grown around the Pt wire, conductivity might be measured as a function of crystal orientation.

To obtain a value of thermal conductivity at a particular temperature, temperatures are allowed to stabilize for 20 min or more. Using a constant current, $\tilde{V}_{3\omega}$ is measured at a series of frequencies and converted to temperature amplitude $\tilde{T}$ using Eq. (1). Typical results are shown in Fig. 129.61(a) for solid D_2, in Fig. 129.61(b) for liquid D_2, and in Fig. 129.61(c) for D_2 gas. Each pair of data points requires 20 to 60 s of averaging, which is performed by a LabVIEW[28] program. The variance in a typical averaged data point is usually consistent with the noise figure (4 nV/Hz$^{1/2}$) of the first stage of amplification.[19] The data in Fig. 129.61 are fitted, using the numerical model, varying only the thermal conductivity of the D_2. It is verified experimentally that the temperature amplitude is proportional to the power dissipated in the Pt wire, so the drive current is maximized (but without noticeably raising the ambient temperature measured on the chamber) to reduce the relative importance of amplifier noise.

For Figs. 129.61(a) and 129.61(b), the numerical model fits the in-phase data very closely from 1 Hz to >1000 Hz, while fitting the out-of-phase data over a smaller frequency range, ~8 Hz to ≥300 Hz. This is typical of many data sets. The reasons for the departures from the fit outside these frequency ranges are not known. Several authors[8,9] use the fitting process to also obtain the specific heat of the medium. This does not work for solid D_2 since varying the specific heat from the literature value simply requires a different value of thermal conductivity to fit the data. This is confirmed by the discussion in Ref. 9 that gives the range of parameters required for sensitivity to specific heat. The data obtained in this study are at frequencies too low to obtain specific heat values.

Data for D_2 gas around the Pt wire show acceptable qualitative fits, as seen in Fig. 129.61(c). As expected, the smaller thermal conductivity of the gas yields much greater thermal amplitudes and the curves differ in shape from those of liquid and solid. In this case, much of the heat dissipated in the Pt wire is conducted along the wire to the ends. To use this method to measure the thermal conductivity of a gas would require extra care in establishing the temperature of the Cu blocks at the ends of the Pt wire, and a greater distance from the wire to other parts of the apparatus would be helpful. Additional discussion of the data for D_2 gas and similar data for vacuum, including temperature profiles along the wire and in the gas, is presented in Ref. 27.

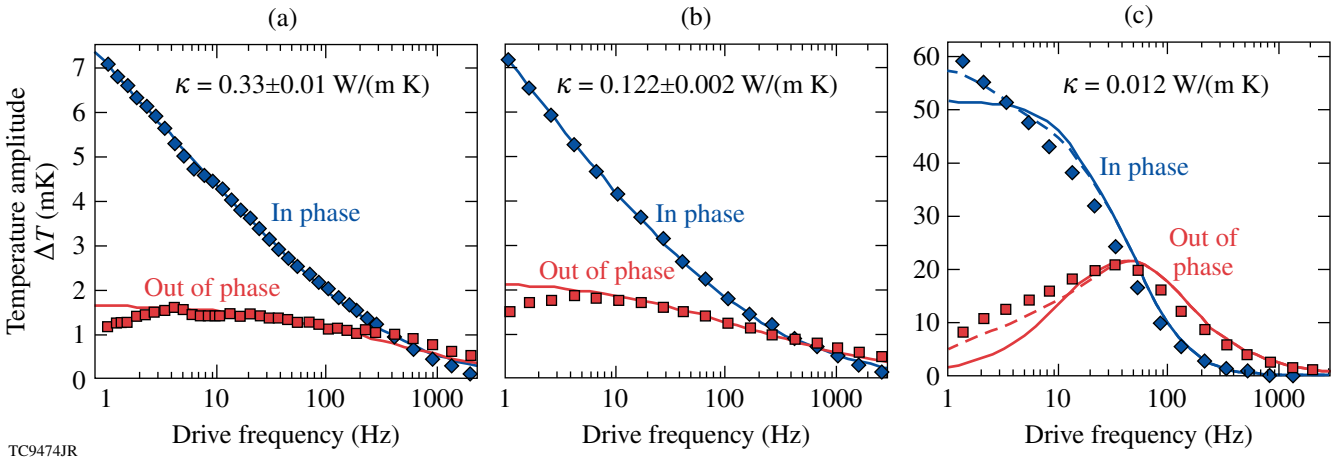

Figure 129.61
Measured (points) and calculated (lines) in-phase and out-of-phase temperature amplitudes of the wire as a function of drive frequency for (a) solid D_2 at 18.2 K with a power dissipation of 45 μW, (b) liquid D_2 at 26 K with a power dissipation of 10 μW, and (c) D_2 gas at 21 K with a pressure of 21 Torr and a power dissipation of 10 μW. (The negative of out-of-phase values is shown.) Fits were obtained by treating only the thermal conductivity κ as a variable. In (c) the fit is qualitative. The effect of choosing the distance to the simulation boundary to be 1 mm (solid lines) or 3 mm (dashed lines) is seen to be significant at low frequencies.

A summary of results for solid D_2 is shown in Fig. 129.62 (solid points). These include data taken for ortho D_2 and instances in which the growth direction of the solid was aligned either with the Pt wire or perpendicular to it. These data are fitted with a second-order polynomial $\kappa = (6.168 - 0.0635\,T + 0.0173\,T^2)$ W/(m K), where T is in units of K. No difference is seen among these data sets. This partially addresses a concern that directionality of crystal growth in the ICF fuel layer could affect the thermal conductivity across the layer and, therefore, the final profile of the layer. The data indicate that ortho-conversion would be an ineffective method, at temperatures between 14 K and the triple point, for altering the conductivity of a fuel layer. The data obtained here are consistent with the published data from Daney[14] and Gorodilov[29] (open symbols), but with the conductivities on average 5% larger than those of Daney. Some data are obtained at lower temperatures than is possible using Daney's method. At the lower temperatures shown in Fig. 129.62, increased thermal conductivity along with reduced resistance of the Pt wire results in lower voltages and the increasing importance of amplifier noise. At these lower temperatures, a longer time is required for the solid D_2 to recover from the stresses that result from shrinkage caused by temperature change. As a result, data are increasingly more difficult to obtain as the temperature is lowered.

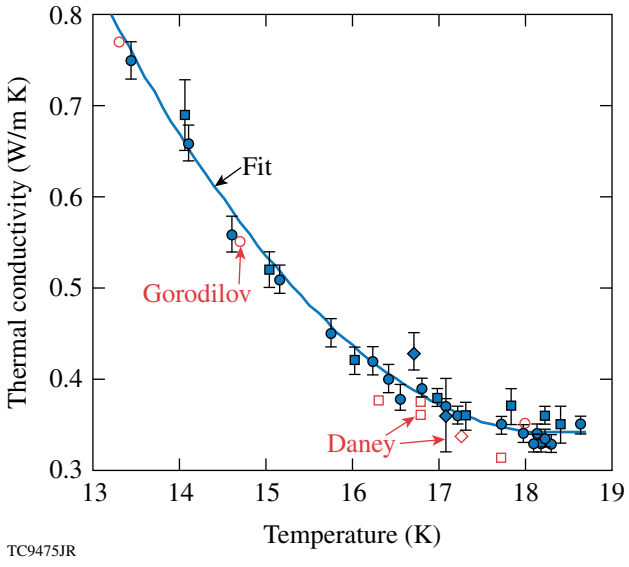

Figure 129.62
Measured values of thermal conductivity of solid D_2 as a function of temperature (solid blue data points). Solid circles are for normal D_2 with the wire parallel to the direction of ice growth. Solid squares (diamonds) are for ortho D_2 with the wire parallel (perpendicular) to the direction of ice growth. The curve is a second-order polynomial fit to the data. Shown for comparison are the data of Daney (open squares for normal D_2 and open diamonds for ortho D_2) and the data of Gorodilov (open circles).

Conclusions

The 3ω method has obtained accurate values of thermal conductivity for solid D_2 in a temperature range lower than any for which it has previously been used. The method operates on a small distance scale appropriate for ICF fuel layers and is somewhat less susceptible to concerns about thermal contraction and formation of cavities than conventional methods of measuring thermal conductivity. Values of thermal conductivity are slightly higher (5%) than those obtained by Daney. The results are all from "good" ice that is free of visible features like cracks and that shows large single crystals when viewed in polarized light. Normal D_2 and ortho D_2 show the same values of thermal conductivity over the temperature range examined. This confirms that ortho-conversion cannot be used at these temperatures as a tool for altering fuel-layer formation. No dependence of thermal conductivity on the direction of solid growth was detected.

ACKNOWLEDGMENT

This work was supported by the U.S. Department of Energy Office of Inertial Confinement Fusion under Cooperative Agreement No. DE-FC52-08NA28302, the University of Rochester, and the New York State Energy Research and Development Authority. The support of DOE does not constitute an endorsement by DOE of the views expressed in this article.

REFERENCES

1. D. R. Harding, D. D. Meyerhofer, S. J. Loucks, L. D. Lund, R. Janezic, L. M. Elasky, T. H. Hinterman, D. H. Edgell, W. Seka, M. D. Wittman, R. Q. Gram, D. Jacobs-Perkins, R. Early, T. Duffy, and M. J. Bonino, Phys. Plasmas **13**, 056316 (2006).
2. J. K. Hoffer and L. R. Foreman, Phys. Rev. Lett. **60**, 1310 (1988).
3. P. S. Ebey, J. M. Dole, D. A. Geller, J. K. Hoffer, J. Morris, A. Nobile, J. R. Schoonover, D. Wilson, M. Bonino, D. Harding, C. Sangster, W. Shmayda, A. Nikroo, J. D. Sheliak, J. Burmann, B. Cook, S. Letts, and J. Sanchez, Fusion Sci. Technol. **54**, 375 (2008); A. S. Bozek *et al.*, Fusion Eng. Des. **82**, 2171 (2007).
4. E. L. Alfonso, I. Anteby, and D. R. Harding, Fusion Technol. **38**, 149 (2000).
5. B. J. Kozioziemski *et al.*, Fusion Sci. Technol. **59**, 14 (2011).
6. B. J. Kozioziemski *et al.*, J. Appl. Phys. **105**, 093512 (2009).
7. D. G. Cahill, Rev. Sci. Instrum. **61**, 802 (1990); erratum **73**, 3701 (2002).
8. N. O. Birge and S. R. Nagel, Rev. Sci. Instrum. **58**, 1464 (1987).
9. F. Chen *et al.*, Rev. Sci. Instrum. **75**, 4578 (2004).
10. L. Lu, W. Yi, and D. L. Zhang, Rev. Sci. Instrum. **72**, 2996 (2001).
11. C. Dames and G. Chen, Rev. Sci. Instrum. **76**, 124902 (2005).

12. G. W. Collins *et al.*, Phys. Rev. B **41**, 1816 (1990).

13. P. C. Souers, *Hydrogen Properties for Fusion Energy* (University of California Press, Berkeley, CA, 1986), pp. 78–80.

14. D. E. Daney, Cryogenics **11**, 290 (1971); D. E. Daney, W. G. Steward, and R. O. Voth, National Bureau of Standards, Washington, DC, NBSIR 73-339 (October 1973).

15. T. Norimatsu *et al.*, J. Vac. Sci. Technol. A **6**, 3144 (1988).

16. D. E. Daney and E. Mapoles, Cryogenics **27**, 427 (1987).

17. Goodfellow Corporation, Berwyn, PA 19312-1780.

18. V. Arp, METALPAK™ software version 1.10, Horizon Technologies, Littleton, CO, 80128; using data from R. J. Corruccini and J. J. Gniewek, *Specific Heats and Enthalpies of Technical Solids at Low Temperatures*, National Bureau of Standards, Monograph 21 (U.S. Government Printing Office, Washington, DC, 1960).

19. Stanford Research Systems, Inc., Sunnyvale, CA 94089.

20. P. C. Souers, *Hydrogen Properties for Fusion Energy* (University of California Press, Berkeley, CA, 1986), p. 79.

21. *ibid.*, 68 and 96.

22. K. Clusius and E. Bartholomé, Z. Phys. Chem. Abt. B **30**, 237 (1935).

23. Sigma-Aldrich, St. Louis, MO 63178.

24. P. C. Souers, *Hydrogen Properties for Fusion Energy* (University of California Press, Berkeley, CA, 1986), pp. 315–316.

25. A. Jacquot *et al.*, J. Appl. Phys. **91**, 4733 (2002).

26. D. S. Kershaw, J. Comput. Phys. **26**, 43 (1978).

27. A. She, *2007 Summer Research Program for High School Juniors at the University of Rochester's Laboratory for Laser Energetics*, University of Rochester, Rochester, NY, LLE Report No. 353, LLE Document No. DOE/SF/19460-809 (2008).

28. National Instruments Corporation, Austin, TX 78759-3504.

29. B. Ya. Gorodilov *et al.*, Sov. J. Low Temp. Phys. **7**, 208 (1981).